Petroleum Science 21 (2024) 3547–3557

Contents lists available at ScienceDirect

Petroleum Science

journal homepage: www.keaipublishing.com/en/journals/petroleum-science

Original Paper

In-situ laboratory study on influencing factors of pre-SC-CO_2 hybrid fracturing effect in shale oil reservoirs

Yu-Xi Zang [a], Hai-Zhu Wang [a], Bin Wang [a], Yong-Gang Yi [c], Tian-Yu Wang [a], Ming-Liang Shi [a], Gang-Hua Tian [a], Shou-Ceng Tian [a, b, *]

[a] State Key Laboratory of Petroleum Resources and Prospecting, China University of Petroleum (Beijing), Beijing, 102249, China
[b] College of Petroleum, China University of Petroleum-Beijing at Karamay, Karamay, 834000, Xinjiang, China
[c] Engineering Technology Research Institute of Xinjiang Oilfield Company, Karamay, 834000, Xinjiang, China

ARTICLE INFO

Article history:
Received 18 November 2023
Received in revised form
23 May 2024
Accepted 25 May 2024
Available online 25 May 2024

Edited by Jia-Jia Fei and Min Li

Keywords:
Pre-CO_2 hybrid fracturing
Fracture propagation
Fracture pattern
Shale oil reservoir

ABSTRACT

Supercritical CO_2 (SC-CO_2) fracturing, being a waterless fracturing technology, has garnered increasing attention in the shale oil reservoir exploitation industry. Recently, a novel pre-SC-CO_2 hybrid fracturing method has been proposed, which combines the advantages of SC-CO_2 fracturing and hydraulic fracturing. However, the specific impacts of different pre−SC-CO_2 injection conditions on the physical parameters, mechanical properties, and crack propagation behavior of shale reservoirs remain unclear. In this study, we utilize a newly developed "pre-SC-CO_2 injection → water-based fracturing" integrated experimental device. Through experimentation under in-situ conditions, the impact of pre-SC-CO_2 injection displacement and volume on the shale mineral composition, mechanical parameters, and fracture propagation behavior are investigated. The findings of the study demonstrate that the pre-injection SC-CO_2 leads to a reduction in clay and carbonate mineral content, while increasing the quartz content. The correlation between quartz content and SC-CO_2 injection volume is positive, while a negative correlation is observed with injection displacement. The elastic modulus and compressive strength exhibit a declining trend, while Poisson's ratio shows an increasing trend. The weakening of shale mechanics caused by pre-injection of SC-CO_2 is positively correlated with the injection displacement and volume. Additionally, pre-injection of SC-CO_2 enhances the plastic deformation behavior of shale, and its breakdown pressure is 16.6% lower than that of hydraulic fracturing. The breakdown pressure demonstrates a non-linear downward trend with the gradual increase of pre-SC-CO_2 injection parameters. Unlike hydraulic fracturing, which typically generates primary fractures along the direction of the maximum principal stress, pre-SC-CO_2 hybrid fracturing leads to a more complex fracture network. With increasing pre-SC-CO_2 injection displacement, intersecting double Y-shaped complex fractures are formed along the vertical axis. On the other hand, increasing the injection rate generates secondary fractures along the direction of non-principal stress. The insights gained from this study are valuable for guiding the design of preSC-CO_2 hybrid fracturing in shale oil reservoirs.

1. Introduction

Over the past century, China's petroleum industry exploration practices have consistently shown that onshore stratum remains the primary resource and serves as the principal foundation for both exploration and development efforts (Zou and Zhu, 2019). China boasts substantial continental shale oil resources, with verified geological reserves of approximately 6.24 × 10^8 t, accounting for 90% of the entire onshore oil reserves (Hu et al., 2020; Wang et al., 2022). Shale oil constitutes a significant substitute resource that plays a crucial role in guaranteeing China's oil security. To achieve efficient and large-scale development of shale reservoirs, hydraulic fracturing has been a popular technique, leading to significant breakthroughs in early-stage shale gas development (Lampe and Stolz, 2015). However, this method also presents certain drawbacks, including high water consumption, low flowback rates, and substantial damage to water-sensitive reservoirs (Warpinski et al., 2009).

* Corresponding author. State Key Laboratory of Petroleum Resources and Prospecting, China University of Petroleum (Beijing), Beijing, 102249, China.
E-mail address: tscsydx@163.com (S.-C. Tian).

https://doi.org/10.1016/j.petsci.2024.05.020

To overcome these concerns, recent research efforts have focused on developing anhydrous fracturing fluids, with SC-CO_2 emerging as a promising alternative to water-based fracturing fluids. SC-CO_2 possesses a range of beneficial characteristics, including low viscosity, excellent fluidity, and extremely low surface tension. After immersion in supercritical CO_2, new cracks and pores appeared in the rock due to the dissolution of minerals (Li et al., 2022). Moreover, it can reduce the pressure required to fracture rocks andthe volume of rock fractured by $ScCO_2$ is several times larger than that of hydraulic fracturing, making it an ideal choice for stimulating unconventional reservoirs (Wang et al., 2020; Zhou et al., 2019). However, the field development results in the oil industry suggest that using SC-CO_2 as the only fracturing fluid for reservoir stimulation is not an ideal approach, as its low viscosity and limited sand-carrying ability lead to suboptimal results (Mojid et al., 2021; Zheng et al., 2022).

In recent years, CO_2 has been frequently used as a pre-fracturing fluid combined with water-based fracturing fluids to achieve optimal fracturing effects in field operations. The primary concept behind this approach is injecting high-pressure CO_2 into the reservoir to create a fracture network, thereby maintaining reservoir pressure and preventing fluid flow blockages in the fractures. Or inject SC-CO_2 at a low discharge rate to weaken the mechanical properties of the reservoir. Subsequently, a water-based fracturing fluid containing proppants is introduced into the reservoir to prop open the fractures, enabling the release of hydrocarbons (Ribeiro et al., 2022). The pre-CO_2 hybrid fracturing method has been successfully applied in various field operations, including the Yanchang Oilfield (Xiao et al., 2022), the Daqing oilfield (Sun et al., 2020), the Changqing oilfield, the Xinjiang oilfield (Yi et al., 2022), the Dagang Oilfield (Sun et al., 2020). This method has displayed significant potential for enhancing production rates in unconventional reservoirs. During the hybrid fracturing process, specific physical and chemical reactions occur between the pre-injected SC-CO_2 and formation fluids, which can influence shale wettability, micro-pore structure, and mechanical properties (Wang et al., 2018). Ultimately, these factors can impact the imbibition of reservoir fluids and subsequent water-based fracturing, thereby affecting the productivity of shale oil reservoirs (Ao et al., 2020). Consequently, a comprehensive investigation into the effects of pre-injecting SC-CO_2 on the mechanical characteristics of shale reservoirs is essential before proceeding with hybrid fracturing.

Up to the present time, a significant cohort of academics has undertaken investigations on the interaction mechanism between SC-CO_2 and host rocks. Lu et al. (2022) employed X-ray computed tomography (CT), low-pressure nitrogen gas adsorption (N_2GA), mercury intrusion porosimetry (MIP), and field emission scanning electron microscopy (FE-SEM) to analyze the SC-CO_2-slick-water coupling effect on the shale pore structure. Memon et al. (2022) conducted SC-CO_2 fracturing tests on cubic shale samples by true triaxial stress cell (TTSC), and quantitative evaluation of rock characteristics by CT imaging and N2GA. Li et al. (2021) analyzed the effect of SC-CO_2 on pores and rock minerals through nuclear magnetic resonance (NMR), X-ray-diffraction (XRD), and SEM experiments. Zhang K. et al. (2021) investigated changes in caprock pore-fracture structure, permeability and mechanical strength under SC-CO_2-H_2O environment by using a high-temperature and high-pressure airtight reaction platform. Chen et al. (2021) used N_2/CO_2 adsorption and XRD methods to quantitatively evaluate the changes in pore structure and mineral content of lignite, bituminous coal and anthracite coal after exposure to SC-CO_2 fluid. Fatah et al. (2021) treated the Eagle Ford and Mancos shale samples with SC-CO_2 at 70 °C and 18 MPa for 30 days, and evaluated the geochemical interaction by XRD, SEM, Fourier Transform Infrared Spectroscopy (FTIR) method. As mentioned above, SC-CO_2 has a significant impact on the physical characteristics of shale through three primary mechanisms: (1) extraction of shale organic matter by SC-CO_2, (2) the reaction between SC-CO_2 and reservoir fluid, leading to the formation of carbonic acid and subsequent shale mineral reactions, and (3) adsorption of CO_2 by the shale matrix mineral, resulting in changes in the potential energy of the shale surface. Currently, most laboratory experimental research methods utilize static immersion experimental devices, immersing powdered shale samples in an SC-CO_2 environment. However, this approach does not allow for the examination of the effects of physical and chemical reactions on shale's mechanical properties. Moreover, the main focus of the aforementioned studies is on CO_2 sequestration, which entails relatively long CO_2 exposure times, while in shale fracturing operations, formations are exposed to CO_2 for relatively short periods. In summary, the fundamental mechanism of the effect of pre-SC-CO_2 injection on changes in mechanical properties during the process of shale hybrid fracturing remains unclear.

At present, on-site fracturing in oilfields mostly relies on experience and lacks corresponding theoretical basis. To address this problem, we develop a novel "pre-SC-CO_2 injection → water-based fracturing" integrated experimental device. This research is carried out in two distinct steps: i) First, simulate the process of pre-SC-CO_2 injection into the reservoir, and use small-sized cores (25 × 50 mm) to investigate the effects of engineering parameters such as pre-SC-CO_2 injection displacement and injection volume. The influence of the basic mechanical properties of the layer is quantitatively evaluated by uniaxial compression test, uniaxial tensile test and other methods; ii) In the second part, we simulate the pre-SC-CO_2 hybrid fracturing process by employing large-scale cores (50 × 100 mm) to study the fractures propagation under various engineering parameters. This study analyzes the mechanism of action of SC-CO_2-shale and discusses its subsequent impact on the development of hybrid fracturing. The aim is to provide theoretical guidance for the development of oilfield shale reservoirs.

2. Experimental methodology

2.1. Specimen preparation

The rock samples used in the experiment came from a typical shale oil formation in China. To ensure the consistency of mechanical properties, all samples are taken from a shale layer in the Bohai Bay Basin at a depth of 2920–2990 m (Fig. 1(a)). For the basic mechanical property measurement experiment (Fig. 1(b)), the samples are cut into cylinders with a diameter of 25 mm and a height of 50 mm using a computer numerical control (CNC) sand wire cutting machine. For the triaxial hydraulic fracturing experiment, cylinders with a diameter of 50 mm and a height of 100 mm are employed (Fig. 1(c)). To avoid stress concentration during the experiment, both sections of the samples are ground flat, ensuring the vertical deviation does not exceed 0.05°. Moreover, to simulate the wellbore, an injection hole with a diameter of 9 mm and a length of 45 mm is drilled at the center of the top circle of the larger sample. A high-strength stainless steel tube with an outer diameter of 8 mm and a length of 35 mm is fixed to the eyelet using epoxy adhesive, leaving a 10 mm open-hole section. To achieve optimal sealing, the samples are placed at a constant temperature for 48 h prior to the test. This process aimed to ensure the best sealing effect for accurate experimental results.

The shale sample powders are tested by XRD (Siemens D5000, Germany). D5000 X-ray Diffraction equipment fitted with a cobalt X-ray tube is used to test 200 mesh powder samples to determine the shale mineral composition before SC-CO_2 injection. Meanwhile,

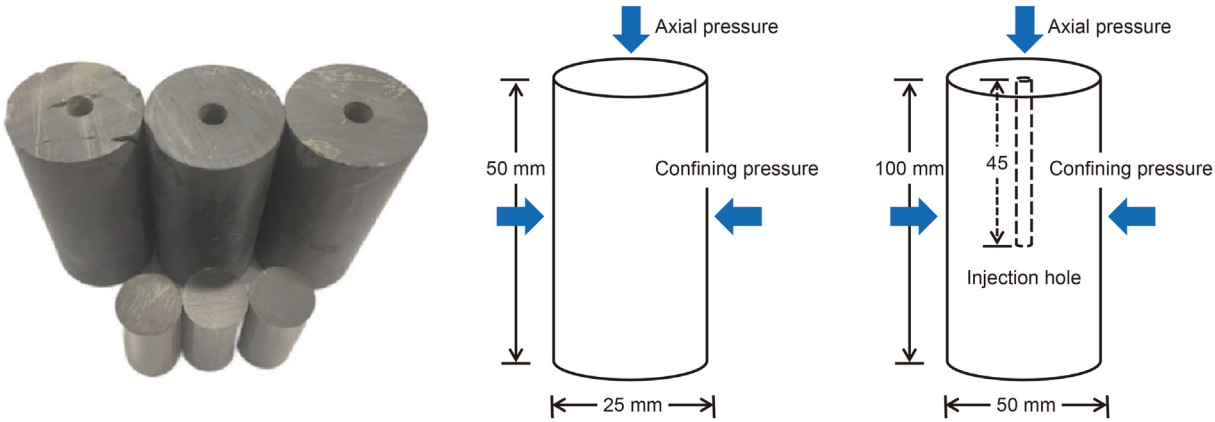

Fig. 1. Rock sample preparation.

the basic mechanical properties of shale samples, including elastic modulus (E_s), Poisson's ratio, compressive strength, and tensile strength are obtained through the uniaxial tensile and compression experiments. Three sets of parallel tests are carried out for each parameter test, and the average values of the parameters are shown in Table 1.

2.2. Experiment apparatus

The independently developed experimental system, as depicted in Fig. 2(a), comprises six sub-modules: gas source supply (such as CO_2, N_2), water source supply, data control device, constant temperature water bath, three-axis servo control, and data acquisition. This system is capable of conducting fracturing experiments involving different fluids. Notably, the maximum pressure of the plunger pump is 50 MPa, which can be combined with the water bath system to control the temperature and pressure of CO_2, enabling the alteration of CO_2's phase state to either a liquid or supercritical state. The data control device operates the motor and vacuum pump while simultaneously recording the changes in pressure and temperature over time using the data acquisition device. The pressure sensor has a measurement range of 0–50 MPa with an accuracy of ±0.1 MPa, while the temperature sensor has a measurement range of 0–80 °C with an accuracy of ±0.1 °C.

The device's innovation lies in its capability to in-situ conduct an integrated "pre-SC-CO_2 injection → water-based fracturing" experiment. The triaxial core support serves as a pivotal component of the fracturing system, enabling core clamping and application of axial pressure and confining pressure. This integral part is constructed entirely from stainless steel, making it suitable for high-temperature and high-pressure experimental conditions, thus facilitating triaxial fracturing experiments at a depth of 5000 m (150 °C, 50 MPa). The core holder is designed to accommodate cylindrical specimens measuring either 25 mm in diameter and 50 mm in height or 50 mm in diameter and 100 mm in height. The triaxial core holder is meticulously designed to accommodate two distinct loading modes: rigid loading and flexible loading. Under the rigid loading mode, the core holder can withstand a maximum axial pressure of 40 MPa and a maximum confining pressure of 50 MPa. This design impeccably fulfills the specifications for specimens subjected to diverse experimental conditions. Both upper and lower ends of the holder are sealed with stainless steel end caps. These end caps feature one or two connecting holes on their respective sides, which enable the injection and discharge of fracturing fluid. To ensure sealing of the sample's side wall and allow for the application of confining pressure, the core sample is enveloped in a Buna rubber cartridge. The application of axial pressure and confining pressure to the core is achieved through a manual hydraulic cylinder, employing a multi-directional synchronous stress loading method. This experimental setup thus enables the realization of the integrated "pre-SC-CO_2 injection → water-based fracturing" experiment, presenting opportunities for conducting comprehensive investigations in shale reservoir fracturing.

Table 1
Mechanical properties of the specimens.

Parameters	Technique	Values
Elastic modulus, GPa	Uniaxial tensile test	17.42
Poisson's ratio, -	Uniaxial tensile test	0.154
Tensile strength, MPa	Uniaxial tensile test	3.67
Compressive strength, MPa	Uniaxial compression test	220.12

2.3. Experimental procedure

The entire experimental process consists of five steps (Fig. 3):

(1) Sample preparation. Cut the experimental sample to a suitable size, and place the sample at a constant temperature for 48 h to achieve the optimal sealing effect.
(2) Stress loading. The cylindrical core is positioned within the newly designed core holder, which is pressurized axially and circumferentially by the manual hydraulic pump. Furthermore, to ensure a consistent and stable SC-CO_2 injection with a fixed displacement, a separate manual hydraulic pump is employed to apply back stress during the pre-SC-CO_2 injection stage.
(3) SC-CO_2 generation. The gaseous CO_2 is pressurized and heated to 7.5 MPa and 40 °C through the plunger pump and the water bath to reach the supercritical state. Since the pipeline of the equipment in this study is short and the pipeline is covered with insulation tape, the pressure and temperature drops of CO_2 during the experiment are negligible, allowing CO_2 to maintain its supercritical state.
(4) Hydraulic fracturing. This step is divided into two stages:
   i) Pre-injection of SC-CO_2. Open Valve 1 and close Valve 2. SC-CO_2 is uniformly injected from the bottom of the rock

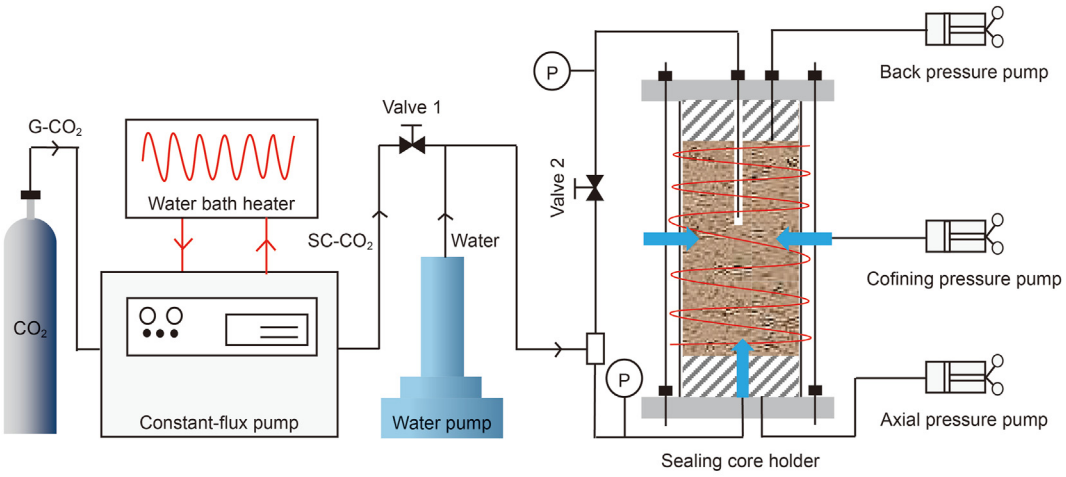

(a) Schematic diagram of the SC-CO_2 pre-injection experimental setup

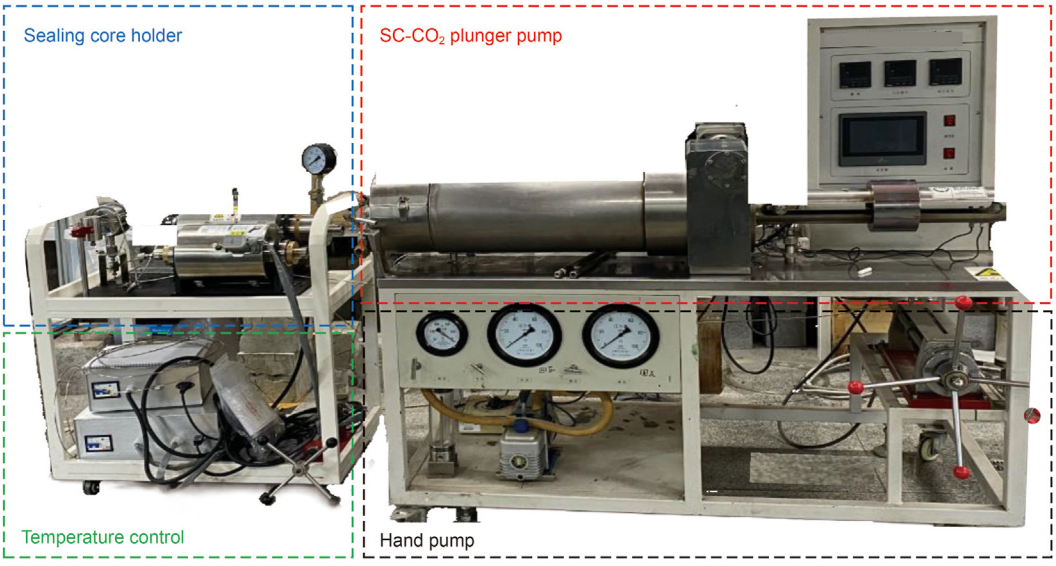

(b) Photograph of the experimental equipment

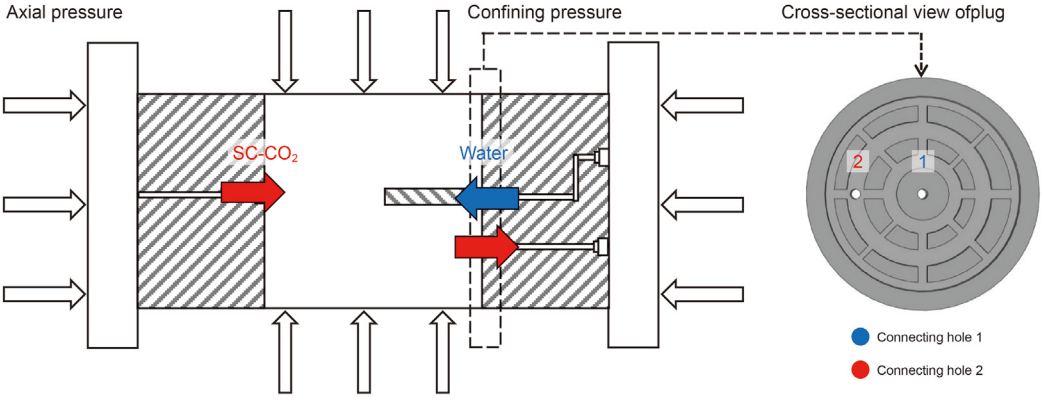

(c) Schematic diagram of core holder

Fig. 2. SC-CO_2 delivery and flow-through equipment.

sample, and the red Connecting hole 2 displayed in Fig. 2(c) serves as the CO_2 discharge end. The stable injection of SC-CO_2 is considered achieved when the pressure gauge reading aligns with the injection pressure of the constant flow pump and stabilizes for a specific duration;

ii) Water-based fluid fracturing. Close Valve 1 and open Valve 2. Activate the ISCO injection pump (Tele-dyne

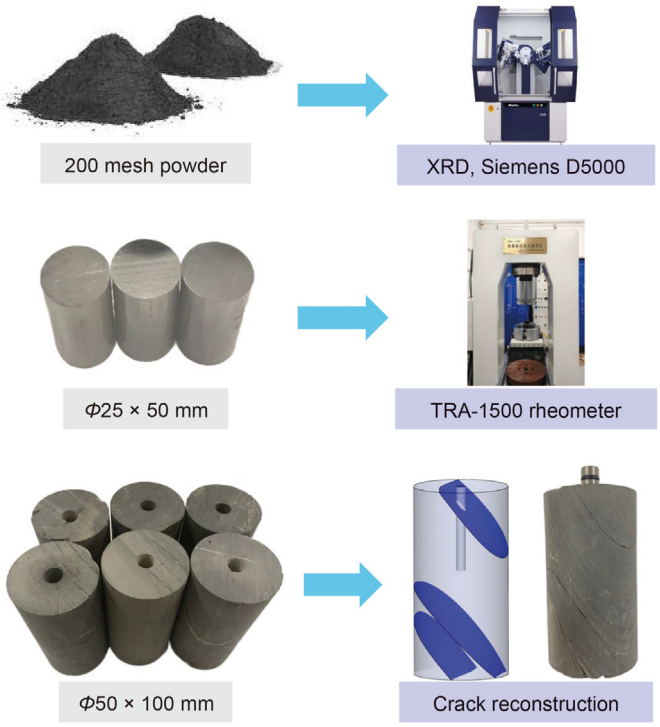

Fig. 3. Experimental sample size and test method.

ISCO, Inc. USA) to pump water-based fracturing fluid into the wellbore through the blue Connecting hole 2. The hydraulic fracturing process is considered complete when a sudden drop in the pressure gauge is observed.

(5) Data collection and analyze. After the above treatment, the core samples undergo a 48-h drying period in a regulated drying oven set at 80 °C. Subsequently, rock samples measuring $\Phi 25 \times 50$ mm are subjected to a comprehensive evaluation of basic mechanical properties using triaxial compression equipment. Simultaneously, rock samples measuring $\Phi 50 \times 100$ mm post-hybrid fracturing undergo a comparative analysis to assess crack reorganization. To delve into changes in mineral composition, the crushed rock samples resulting from the fracturing process are finely processed into 200 mesh powder for subsequent XRD testing.

2.4. Experimental scheme

The primary objective of this study is to propose the advantages of pre-SC-CO_2 hybrid fracturing, and quantitatively analyze the influence of engineering parameters, such as pre-SC-CO_2 injection displacement and injection volume, on the expansion of fracturing fractures. To design the experimental setups, we consider the reservoir block conditions and relevant fracturing construction experience reported in previous literature (Tian et al., 2021; Li et al., 2020). The confining stress is set at 15 MPa, and the axial stress is determined to be 10 MPa. Utilizing the principles of orthogonal testing, we formulate eleven distinct schemes, as presented in Table 2. Among these schemes, Samples #1–3, Samples #2, 4, 5 respectively analyze the influence of pre-SC-CO_2 injection displacement and injection volume on the mineral composition and mechanical properties of shale; Samples #6–8, Samples # 7, 9, 10 respectively consider the impact of pre-SC-CO_2 injection displacement and injection volume on the expansion of hybrid fracturing fractures. Furthermore, we compare and analyze the effect of employing single water-based fracturing fluid (Sample #11) for comparative evaluation.

Among these schemes, to establish a correlation between the field prototype and the experimental model, the pressure loaded and the injection parameters are determined based on the similarity criterion (Eq. (1)) used in hydraulic fracturing simulation experiments (Liu et al., 2000). It is noteworthy that in pre-construction SC-CO_2 injection in oilfields, both domestic and international practices do not consider fracture creation, hence the injection displacement is relatively low, approximately 2–4 m^3/min (Xiao et al., 2022; Ribeiro et al., 2022). Consequently, the injection displacement chosen for this experimental simulation is set to range from 0.05 to 0.2 mL/min.

$$\begin{cases} \dfrac{c_L^3}{c_Q c_T} = 1, c_{K_L}\sqrt{\dfrac{c_L}{c_Q}} = 1, \dfrac{c_\eta c_Q}{c_L^3 c_p} = 1 \\ \dfrac{c^0_{\sigma_{zz}}}{c_E} = \dfrac{c_p}{c_E} = \dfrac{c_{p_f}}{c_E} = 1 \\ \dfrac{c_L c_E^2}{c^2_{k_{IC}}} = 1, \dfrac{c_\gamma c_L}{c_E} = 1 \end{cases} \tag{1}$$

Among them, the similarity ratio coefficient, denoted as $c_V = V_{\text{model}}/V_{\text{field}}$, signifies the ratio of the same physical quantity between the model and the prototype. Here, V represents various single-valued conditional quantities, including L (length, m), E (Young's modulus, GPa), Q (flow rate, m^3/min), T (temperature, °C), K_L (leak-off coefficient, m/$\sqrt{\text{min}}$), η (viscosity, mPa·s), p (pressure, Pa), p_f (fracture pressure, Pa), σ^0_{zz} (confining stress, Pa), γ (shear modulus, Pa), K_{IC} (fracture toughness, MN/$m^{3/2}$), and other relevant parameters.

3. Results and discussion

In this section, we perform XRD tests on shale powder samples both before and after SC-CO_2 injection. Additionally, conduct a comparative analysis of the changes in the mechanical properties under various pre-SC-CO_2 injection displacement and injection volume, based on data obtained from the uniaxial tensile test and uniaxial compressive test. Furthermore, by employing pumping pressure-time curves and fracture recombination, among other methods, we conduct a comparative analysis of fracture propagation characteristics under conditions of hybrid fracturing and single water-based fracturing fluid.

3.1. Changes of mineral composition

Fig. 4 illustrates the impact of pre-SC-CO_2 injection on the mineral composition of shale. XRD analyses of the original rock samples revealed that quartz (20.1%) and clay minerals (31.8%) constituted the predominant minerals, accompanied by calcite (15.8%), dolomite (11.4%), feldspar (4.8%), and other minor components (16.8%). Following pre-SC-CO_2 injection, SC-CO_2 comes into full contact with the shale, leading to changes in the shale's mineral composition (Eq. (2)–(6)) (Li et al., 2021; Yang et al., 2023; Wu et al., 2021). Under various injection displacements, the shale's content of feldspar, calcite, dolomite, and clay minerals decreases by 56.1%, 17.1%, 5.3%, and 2.2%, respectively. Simultaneously, the relative content of quartz experiences an increase of 9.5%. Additionally, under different injection volumes, shale feldspar, calcite, dolomite, and clay minerals decrease by 14.6%, 12.0%, 12.3%, and

Table 2
Experimental schemes.

Sample	Size, mm	Injection displacement, mL/min	Injection volume, PV	Fluid type
# 1/2/3	25 × 50	0.05/0.1/0.15	3	SC-CO_2
# 4/5		0.1	5/7	
# 6/7/8	50 × 100	0.2/0.35/0.5 → 5 (water)	3	SC-CO_2→water
# 9/10		0.35 → 5 (water)	5/7	
# 11		5	–	water

$\sigma_c \times \sigma_a \times \sigma_b = 15 \times 10 \times 8$ MPa (σ_c: confining stress; σ_a: axial stress; σ_b: back stress).

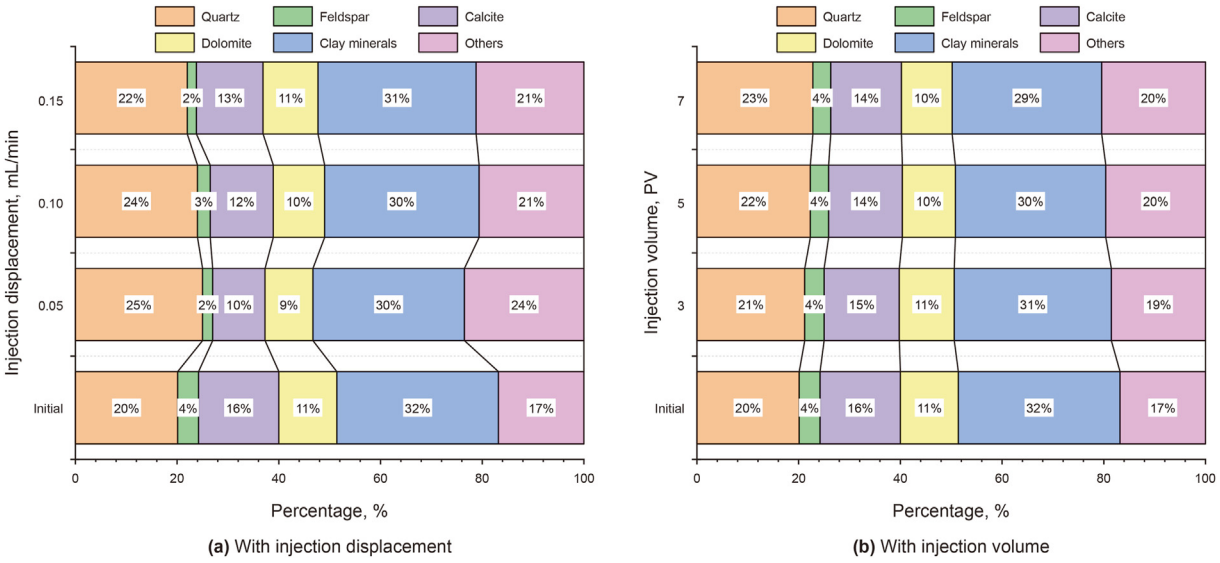

Fig. 4. Mineral content changes under pre-SC-CO_2 injection.

7.5%, respectively, while the relative content of quartz shows a significant increase of 13.4%. Notably, the increment in shale quartz content exhibits a positive correlation with SC-CO_2 injection volume, while it demonstrates a negative correlation with SC-CO_2 injection displacement.

$$CO_2 + H_2O \leftrightarrow H^+ + HCO_3^- \quad (2)$$

$$CaCO_3 + H^+ + HCO_3^- \rightarrow Ca^{2+} + 2HCO_3^- \quad (3)$$

$$CaMg(CO_3)_2 + 2H^+ \rightarrow Ca^{2+} + Mg^{2+} + 2HCO_3^- \quad (4)$$

$$Ca^{2+} + HCO_3^- \rightarrow CaCO_3 + H^+ \quad (5)$$

$$Mg^{2+} + HCO_3^- \rightarrow MgCO_3 + H^+ \quad (6)$$

3.2. Changes of mechanical properties

Fig. 5 presents stress-strain curves for shale samples subjected to different pre-SC-CO_2 injection displacements and injection volumes. The curve can be categorized into four distinct stages: initial linear elastic stage, strain hardening stage, yield stage, and deformation stage (Roylance, 2001). During uniaxial compression, the initial rock sample experienced brittle failure, characterized by a sudden stress peak followed by a rapid decline. However, after pre-injection of SC-CO_2, a significant alteration is observed in the local deformation stage of the shale sample. This change suggests that SC-CO_2 undergoes both physical and chemical reactions with the rock sample, leading to a weakening of its mechanical properties. Consequently, the failure mode shifts from brittle shear failure to plastic failure, as reported in the relevant literature (Memon et al., 2022; Pan et al., 2018; Middleton et al., 2015).

Table 3 presents the changes in the mechanical properties of shale samples before and after SC-CO_2 injection. The extent of damage can be ascertained by comparing the E_s, compressive strength and Poisson's ratio under varying SC-CO_2 injection conditions (Qin et al., 2016). The variations in mechanical properties are found to be closely linked to both the SC-CO_2 injection displacement and injection volume. When subjected to different SC-CO_2 injection displacements, the elastic modulus of shale exhibits a decreasing trend, declining by 4.9%, 11.5%, and 14.5% compared to its initial condition. Additionally, the compressive strength shows a similar downward trend, decreasing by 3.1%, 6.2%, and 7.9% respectively, compared to its initial condition. However, Young's modulus displays an increasing trend, showing increments of 5.2%, 11.0%, and 19.5% compared to its initial condition. Furthermore, when considering various SC-CO_2 injection volumes, the elastic modulus demonstrates reductions of 11.5%, 18.3%, and 26.9% relative to its initial state. Additionally, the compressive strength displays decreases of 6.2%, 8.6%, and 9.2% compared to its initial condition. In contrast, Young's modulus consistently increases under different injection volumes, exhibiting increments of 11.0%, 24.0%, and 32.5%, respectively, compared to its initial condition. The study identifies that continuous SC-CO_2 injection enhanced the dissolution of inorganic minerals within the shale samples, with injection volume exerting a more pronounced effect

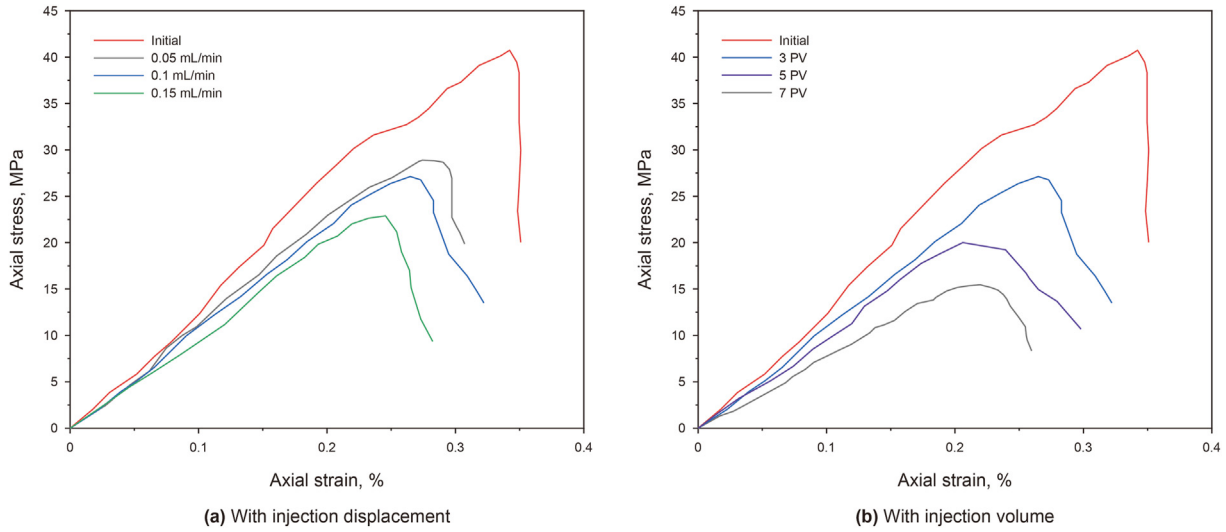

Fig. 5. Stress-strain curves change under pre-SC-CO_2 injection.

Table 3
Mechanical parameters variations under pre-SC-CO_2 injection.

Treatment		E_s, GPa	Compressive strength, MPa	Poisson's ratio, -
–	Initial	17.42	220.12	0.154
Injection displacement, mL/min	0.05	16.56	213.21	0.162
	0.1	15.42	206.57	0.171
	0.15	14.89	202.83	0.184
Injection volume, PV	3	15.42	206.57	0.171
	5	14.24	201.24	0.191
	7	12.74	199.78	0.204

on the mechanical properties. These findings align with previous research trends (Su et al., 2020; Lu et al., 2019; Middleton et al., 2015); however, this research observes a more conspicuous degree of change in mechanical properties. This increased significance can be attributed to the dynamic SC-CO_2 injection process, where the fluid's enhanced fluidity intensifies physical and chemical reactions during the interactions.

3.3. Pumping pressure-injection time curves

In the process of hydraulic fracturing, Fig. 6 illustrates the changes in pumping pressure over time, and the fracture pressure of the formation under different pre-SC-CO_2 injection parameters. All curves can be segmented into three distinct phases: i) the pressure rise phase; ii) the pressure drop phase; iii) the fracture growth and stabilization phase. When an abrupt reduction in

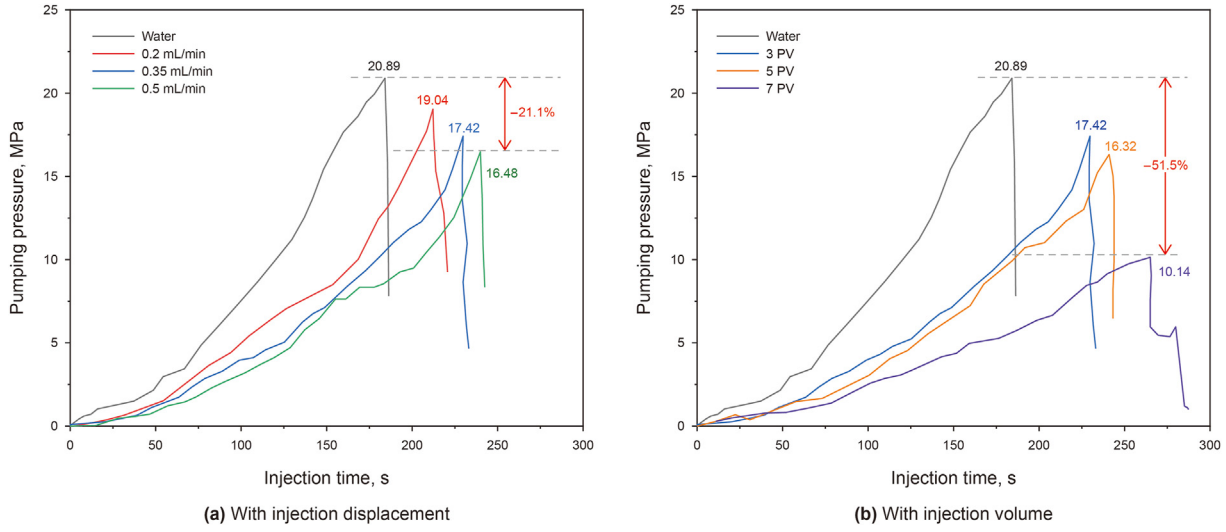

Fig. 6. Pumping pressure-injection time curves change under pre-SC-CO_2 injection.

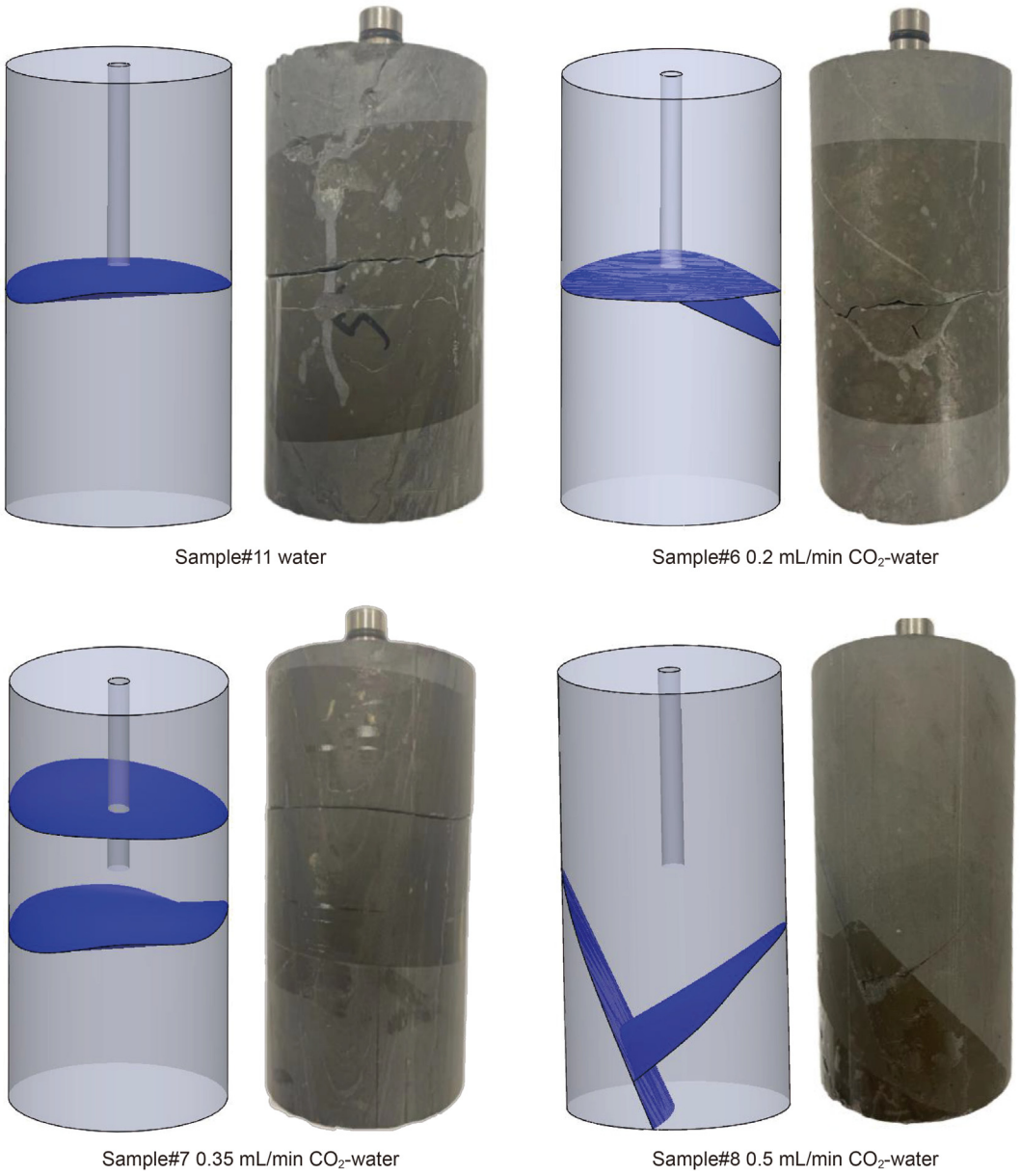

Fig. 7. Schematic diagram of crack reconstruction (water/SC-CO_2 injection displacement).

pumping pressure occurs, it can be inferred that the rock undergoes fracturing at that moment. The maximum pumping pressure prior to the abrupt pressure drop is referred to as the formation breakdown pressure (Zhao et al., 2019).

The advantages of the pre-SC-CO_2 injection hybrid fracturing process become evident when comparing the pumping pressure curves of Sample #7 and #11. It is evident that the pumping pressure curve for hydraulic fracturing rises more rapidly, which can be attributed to the lower compression degree of water-based fracturing fluid compared to SC-CO_2. Additionally, SC-CO_2 exhibits characteristics such as low viscosity and almost zero interfacial tension, leading to significant fluid loss during fracturing. These observations align with findings from previous studies (Zhang C. et al., 2021). It is noteworthy that the breakdown pressure decreases from 20.89 to 17.42 MPa, indicating a reduction of 16.6%.

In the pumping pressure curves present in Fig. 6(a) for various pre-SC-CO_2 injection displacements (Sample #6/7/8), it is evident that the breakdown pressure exhibits a nonlinear decrease with increasing displacement. Specifically, when compared to the condition of 0.2 mL/min displacement, the breakdown pressure at 0.35 and 0.5 mL/min displacements are reduced by 8.5% and 13.4%, respectively. Additionally, it is essential to note that the increase in pumping pressure of pre-SC-CO_2 hybrid fracturing is minimal, and the rate of increase demonstrates a downward trend with the rise of SC-CO_2 injection displacement. Moving on to Fig. 6(b), the pumping curves related to the pre-SC-CO_2 injection volume exhibit a similar trend (Sample #7/9/10). In comparison to the condition of 3 PV, the breakdown pressure is reduced by 6.3% and 41.8% when the injection volume is 5 and 7 PV, respectively. Among these observations, when the initial SC-CO_2 injection volume is 7 PV, the injection pressure exhibits a zigzag pattern during the fracturing process. Notably, when the injection pressure reaches the first peak, a second secondary peak emerges later, indicating the generation of secondary fractures during the propagation of primary fractures.

Fig. 8. Schematic diagram of crack reconstruction (water/SC-CO_2 injection volume).

Building upon the research findings delineated in the previous section of this paper, the observed decline in breakdown pressure can be attributed to three principal factors: (1) Chemical interaction. Pre-injected SC-CO_2 interacts chemically with the reservoir minerals, leading to a downward trend in reservoir mechanical properties (E_s and compressive strength); (2) Micro-fracture introduction: The shale reservoir already contains well-developed bedding and natural fractures. With the continuous injection of low-displacement SC-CO_2, the gas infiltrates the tiny pores within the reservoir. As the local fracture pressure is reached, the reservoir fractures, forming new tiny fractures or connecting with existing natural fractures; (3) Thermal damage: pre-injected high-temperature SC-CO_2 causes thermal damage to the reservoir. Temperature-induced thermal stress plays a significant role in internal rock damage, often leading to the initiation and propagation of cracks (Isaka et al., 2019; Esteves et al., 2019). However, considering the relatively small injection volume of pre-SC-CO_2, the impact of this factor may be limited.

3.4. Fracture propagation characteristics

Owing to the small sample size, the crack distribution and morphology after fracturing can be determined by examining the crack textures on the top, bottom, and sides of the cylinder specimen. Utilizing SolidWorks software (Kurowski, 2013) for internal crack reconstruction, a clear observation of crack development under various working conditions is attainable, as depicted in Figs. 7 and 8. Due to severe cracking of the sample upon removal from the core holder, it is meticulously reassembled using transparent plastic tape. Additionally, to indicate the locations of fractures resulting from hydraulic fracturing, distinct markings are applied using blue color.

The examination of Figs. 7 and 8 reveals that during hydraulic fracturing, main fractures primarily occur along the vertical axis of the sample. In contrast, when pre-SC-CO_2 hybrid fracturing is employed, multiple secondary fractures manifest in the sample, resulting in the formation of a complex fracture network. Given

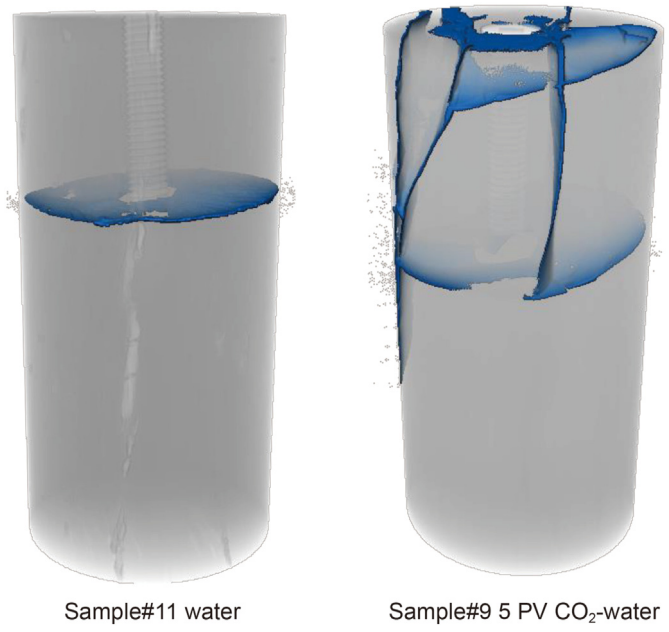

Fig. 9. CT scans of rock samples under different fracturing fluid injection conditions.

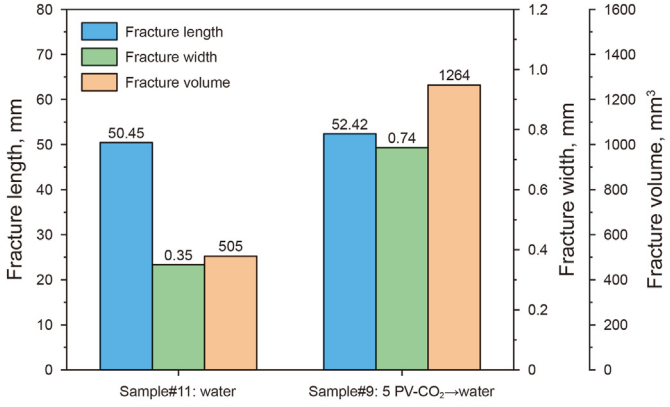

Fig. 10. Fracture size characteristics under different fracturing fluid injection conditions.

that SC-CO_2 readily permeates the minute pores within the rock, it exerts an influence on the internal pore structure of the rock during the pre-injection phase. Consequently, it becomes apparent that certain fractures may be located at a considerable distance from the injection point when conducting hybrid fracturing. The analysis of fracture morphology resulting from water fracturing and pre-CO_2 hybrid fracturing is conducted through image reconstruction (Fig. 9), utilizing CT scanning equipment with the precision of 53 μm (Zeiss). When employing one single water-based fracturing fluid, the average fracture length, fracture width, and fracture volume demonstrated increases from 50.45 to 52.42 mm, 0.35–0.74 mm, and 505–1264 mm^3, respectively. The increments represent a rise of 3.9%, 111.4%, and 150.3%, as illustrated in Fig. 10.

Through comparison, it becomes evident that pre-SC-CO_2 injection parameters significantly influence the formation of fractures during the fracturing process. As illustrated in Fig. 7, when the pre-injected SC-CO_2 injection displacement is low (<0.35 mL/min), the two primary fractures primarily expand in a direction parallel to the maximum principal stress and are located near the perforated wellbore. However, when the SC-CO_2 injection displacement is increased to 0.5 mL/min, the fracture network becomes more intricate, and double Y-shaped cross fractures appear along the direction of the straight axis. Furthermore, based on the fracture structure depicted in Fig. 8, the injected volume of SC-CO_2 emerges as another pivotal parameter influencing fracture propagation. As the injection volume increases, secondary fractures extend along the axial direction progressively. The pre-injected CO_2 rapidly accumulates within the reservoir, leading to a swift increase in the local reservoir pressure and subsequently initiating fracturing cracks. At this juncture, the principal stress ceases to be the dominant factor governing crack initiation and propagation. From the foregoing observations, it is evident that higher pre-SC-CO_2 injection displacement and volume lead to an augmented number and intricacy of fractures compared to those formed under lower injection parameters. With the increase in pre-SC-CO_2 injection parameters, the mechanical properties of the shale are weakened, and the possibility of introducing new micro-fractures rises. Consequently, when subsequent water-based fracturing fluid is injected for hybrid fracturing, the resulting fracture network structure exhibits a heightened level of complexity.

4. Conclusions

By synergizing the benefits of SC-CO_2 and water fracturing, a novel pre-SC-CO_2 hybrid fracturing method has been proposed. Utilizing the newly designed "pre-SC-CO_2 injection → water-based fracturing" integrated experimental device, a comparative analysis of the shale mineral composition, mechanical properties and fracture propagation of different pre-SC-CO_2 injection displacement and injection volumes is conducted. The following conclusions can be drawn:

(1) Pre-SC-CO_2 injection significantly influences the shale mineral composition. The injection of SC-CO_2 results in a reduction of carbonate minerals and clay content in shale, accompanied by an increase in the relative content of quartz. Specifically, the increase in shale quartz content exhibits a positive correlation with SC-CO_2 injection volume but displays a negative correlation with SC-CO_2 injection displacement.

(2) Pre-SC-CO_2 injection initiates physical and chemical reactions with rock samples, leading to a declining trend in elastic modulus and compressive strength. Additionally, the failure mode gradually transitions from brittle shear failure to plastic failure.

(3) The breakdown pressure of the pre-SC-CO_2 hybrid fracturing formation is observed to be 16.6% lower than that of the hydraulic fracturing, underscoring the benefits of employing hybrid fracturing technology. Furthermore, as the displacement and volume of SC-CO_2 injection progressively increase, the breakdown pressure exhibits a nonlinear downward trend.

(4) In contrast to hydraulic fracturing, which generates only main fractures along the direction of the maximum principal stress, pre-SC-CO_2 hybrid fracturing results in the formation of a more intricate and complex fracture network.

CRediT authorship contribution statement

Yu-Xi Zang: Writing – review & editing, Writing – original draft, Software, Methodology, Investigation, Data curation, Conceptualization. **Hai-Zhu Wang:** Writing – review & editing, Methodology, Conceptualization. **Bin Wang:** Supervision, Software. **Yong-Gang Yi:** Supervision. **Tian-Yu Wang:** Writing – review &

editing. **Ming-Liang Shi:** Writing – review & editing. **Gang-Hua Tian:** Writing – review & editing. **Shou-Ceng Tian:** Supervision, Project administration, Conceptualization.

Declaration of competing interest

The authors declare that they have no known competing financial interests or personal relationships that could have appeared to influence the work reported in this paper.

Acknowledgments

This study was funded by Science Foundation of China University of Petroleum, Beijing (No. 2462021YXZZ009) and The Strategic Cooperation Technology Projects of CNPC and CUPB (No. ZLZX 2020–01) and Innovation Capability Support of Shaanxi (Program No. 2023-CX-TD-31) Technical Innovation Team for Low Carbon Environmental Protection and Enhanced Oil Recovery in Unconventional Reservoirs.

References

Ao, X., Qi, Z., Xiang, Z., et al., 2020. Swelling of shales by supercritical carbon dioxide and its relationship to sorption. ACS Omega 5 (31), 19606–19614. https://doi.org/10.1021/acsomega.0c02118.

Chen, K., Liu, X., Wang, L., et al., 2021. Influence of sequestered supercritical CO_2 treatment on the pore size distribution of coal across the rank range. Fuel 306, 121708. https://doi.org/10.1016/j.fuel.2021.121708.

Esteves, A.F., Santos, F.M., Pires, J.C.M., 2019. Carbon dioxide as geothermal working fluid: an overview. Renew. Sustain. Energy Rev. 114, 109331. https://doi.org/10.1016/j.rser.2019.109331.

Fatah, A., Mahmud, H.B., Bennour, Z., et al., 2021. Effect of supercritical CO_2 treatment on physical properties and functional groups of shales. Fuel 303, 121310. https://doi.org/10.1016/j.fuel.2021.121310.

Hu, S., Zhao, W., Hou, L., et al., 2020. Development potential and technical strategy of continental shale oil in China. Petrol. Explor. Dev. 47 (4), 877–887. https://doi.org/10.1016/S1876-3804(20)60103-3.

Isaka, B.A., Ranjith, P., Rathnaweera, T., 2019. The use of super-critical carbon dioxide as the working fluid in enhanced geothermal systems (EGSs): a review study. Sustain. Energy Technol. Assessments 36, 100547. https://doi.org/10.1016/j.seta.2019.100547.

Kurowski, P., 2013. Engineering Analysis with SolidWorks Simulation 2013. SDC publications.

Lampe, D.J., Stolz, J.F., 2015. Current perspectives on unconventional shale gas extraction in the Appalachian Basin. J. Environ. Sci. Health, Part A 50 (5), 434–446. https://doi.org/10.1080/10934529.2015.992653.

Li, L., Chen, Z., Su, Y.L., et al., 2021. Experimental investigation on enhanced-oil-recovery mechanisms of using supercritical carbon dioxide as prefracturing energized fluid in tight oil reservoir. SPE J. 26 (5), 3300–3315. https://doi.org/10.2118/202279-PA.

Li, H., Jiang, X., Xu, Z., et al., 2022. The effect of supercritical CO_2 on failure mechanisms of hot dry rock. Adv. Geo-Energy Res. https://doi.org/10.46690/ager.2022.04.07.

Li, X., Wu, C., Zhao, S., et al., 2020. Technology for cementing shale oil reservoirs in Dagang Oilfield: study and application. Drill. Fluid Complet. Fluid 37 (2), 232–238. https://doi.org/10.3969/i.issn.1001-5620.2020.02.017.

Liu, G., Pang, F., Chen, Z., 2000. Similarity criterion in hydraulic fracturing simulation experiments. J. Univ. Pet., China (Ed. Nat. Sci.) 24 (5), 45–48. https://doi.org/10.3321/j.issn:1000-5870.2000.05.013.

Lu, Y., Chen, X., Tang, J., et al., 2019. Relationship between pore structure and mechanical properties of shale on supercritical carbon dioxide saturation. Energy 172, 270–285. https://doi.org/10.1016/j.energy.2019.01.063.

Lu, Y., Liu, J., Tang, J., et al., 2022. Pore changes of slickwater-containing shale under supercritical CO_2 treatment. Fuel 312, 122775. https://doi.org/10.1016/j.fuel.2021.122775.

Memon, S., Feng, R., Ali, M., et al., 2022. Supercritical CO_2-Shale interaction induced natural fracture closure: implications for $scCO_2$ hydraulic fracturing in shales. Fuel 313, 122682. https://doi.org/10.1016/j.fuel.2021.122682.

Middleton, R.S., Carey, J.W., Currier, R.P., et al., 2015. Shale gas and non-aqueous fracturing fluids: opportunities and challenges for supercritical CO_2. Appl. Energy 147, 500–509. https://doi.org/10.1016/j.apenergy.2015.03.023.

Mojid, M.R., Negash, B.M., Abdulelah, H., et al., 2021. A state-of-art review on waterless gas shale fracturing technologies. J. Petrol. Sci. Eng. 196, 108048. https://doi.org/10.1016/j.petrol.2020.108048.

Pan, Y., Hui, D., Luo, P., et al., 2018. Experimental investigation of the geochemical interactions between supercritical CO_2 and shale: implications for CO_2 storage in gas-bearing shale formations. Energy Fuel. 32 (2), 1963–1978. https://doi.org/10.1021/acs.energyfuels.7b03074.

Qin, L., Zhai, C., Liu, S., et al., 2016. Failure mechanism of coal after cryogenic freezing with cyclic liquid nitrogen and its influences on coalbed methane exploitation. Energy Fuel. 30 (10), 8567–8578. https://doi.org/10.1021/acs.energyfuels.6b01576.

Ribeiro, L., Thoma, A., Bryant, J., et al., 2022. Lessons learned from the large-scale CO_2 stimulation of 11 unconventional wells in the Williston Basin: a practical review of operations, logistics, production uplift, and CO_2 storage. SPE Prod. Oper. 37 (4), 698–709. https://doi.org/10.2118/209159-PA.

Roylance, D., 2001. Stress-strain Curves. Massachusetts Institute of Technology study, Cambridge.

Su, E., Liang, Y., Chang, X., et al., 2020. Effects of cyclic saturation of supercritical CO_2 on the pore structures and mechanical properties of bituminous coal: an experimental study. J. CO_2 Util. 40, 101208. https://doi.org/10.1016/j.jcou.2020.101208.

Sun, Z., Wang, H., Song, L., 2020. A case study of hydraulic fracturing in ordos shale under the combined use of CO_2 and gelled fluid. In: SPE/AAPG/SEG Unconventional Resources Technology Conference. URTEC. Virtual. https://doi.org/10.15530/urtec-2020-2457.

Tian, F., Liu, X., Zhang, S., et al., 2021. Continuous sand fracturing technology with slick water for continental shale oil in the Dagang Oilfield. Petrol. Drill. Tech. 49 (4), 118–124. https://doi.org/10.11911/syztjs.2021021.

Wang, H., Li, G., He, Z., et al., 2018. Experimental investigation on abrasive supercritical CO_2 jet perforation. J. CO_2 Util. 28, 59–65. https://doi.org/10.1016/j.jcou.2018.09.018.

Wang, H., Li, G., Zheng, Y., et al., 2020. Research status and prospects of supercritical CO_2 fracturing technology. Acta Pet. Sin. 41 (1), 116. https://doi.org/10.7623/syxb202001011.

Wang, X., Li, J., Jiang, W., et al., 2022. Characteristics, current exploration practices, and prospects of continental shale oil in China. Adv. Geo-Energy Res. 6 (6), 454–459. https://doi.org/10.46690/ager.2022.06.02.

Warpinski, N.R., Mayerhofer, M.J., Vincent, M.C., et al., 2009. Stimulating unconventional reservoirs: maximizing network growth while optimizing fracture conductivity. J. Can. Petrol. Technol. 48 (10), 39–51. https://doi.org/10.2118/114173-PA.

Wu, Y., Tao, J., Wang, J., et al., 2021. Experimental investigation of shale breakdown pressure under liquid nitrogen pre-conditioning before nitrogen fracturing. Int. J. Min. Sci. Technol. 31 (4), 611–620. https://doi.org/10.1016/j.ijmst.2021.05.006.

Xiao, Y., Li, Z., Wang, J., et al., 2022. Study on enhancing shale oil recovery by CO_2 Pre-Pad energized fracturing in A83 block, ordos basin. Atmosphere 13 (9), 1509. https://doi.org/10.3390/atmos13091509.

Yang, K., Zhou, J., Xian, X., et al., 2023. Effect of supercritical CO_2-water-shale interaction on mechanical properties of shale and its implication for carbon sequestration. Gas Sci. Eng. 111, 204930. https://doi.org/10.1016/j.jgsce.2023.204930.

Yi, Y., Huang, K., Li, J., et al., 2022. Effect of CO_2 pre-pad in volume fracturing of conglomerate reservoirs in Mahu Sag, Junggar Basin. Xinjiang Petrol. Geol. 43 (1), 6. https://doi.org/10.7657/XJPG20220106.

Zhang, C., Liu, S., Ma, Z., Ranjith, P., 2021. Combined micro-proppant and supercritical carbon dioxide ($SC\text{-}CO_2$) fracturing in shale gas reservoirs: a review. Fuel 305, 121431. https://doi.org/10.1016/j.fuel.2021.121431.

Zhang, K., Sang, S., Zhou, X., et al., 2021. Influence of supercritical CO_2-H_2O-caprock interactions on the sealing capability of deep coal seam caprocks related to CO_2 geological storage: a case study of the silty mudstone caprock of coal seam no. 3 in the Qinshui Basin, China. Int. J. Greenh. Gas Control 106, 103282. https://doi.org/10.1016/j.ijggc.2021.103282.

Zhao, X., Huang, B., Xu, J., 2019. Experimental investigation on the characteristics of fractures initiation and propagation for gas fracturing by using air as fracturing fluid under true triaxial stresses. Fuel 236, 1496–1504. https://doi.org/10.1016/j.fuel.2018.09.135.

Zheng, Y., Wang, H., Tian, G., et al., 2022. Experimental investigation of proppant transport in hydraulically fractured wells using supercritical CO_2. J. Petrol. Sci. Eng. 217, 110907. https://doi.org/10.1016/j.petrol.2022.110907.

Zhou, J., Hu, N., Xian, X., et al., 2019. Supercritical CO_2 fracking for enhanced shale gas recovery and CO_2 sequestration: Results, status and future challenges. Adv. Geo-Energy Res. 3 (2), 207–224. https://doi.org/10.26804/ager.2019.02.10.

Zou, C., Zhu, K.L., 2019. Preface for the special issue of formation and enrichment of tight (shale) oil resources in Chinese continental basins. J. Asian Earth Sci. 178, 1–2. https://doi.org/10.1016/j.jseaes.2019.03.016.